Facile electrospinning fabrication and photoluminescence of $La_2O_2S:Tb^{3+}$ nanobelts derived from $La_2O_3: Tb^{3+}$ nanobelts

FEI BI[a], LIYANG WANG[a,*], JIAQI LI[b], GUANGQING GAI[a], XIANGTING DONG[b]

[a]*Laboratory of Building Energy-Saving Technology Engineering, College of Material Science and Engineering, Jilin Jianzhu University, Changchun 130118, China*
[b]*Key Laboratory of Applied Chemistry and Nanotechnology at Universities of Jilin Province, Changchun University of Science and Technology, Changchun 130022, China*

Novel structures of $La_2O_2S:Tb^{3+}$ nanobelts were successfully prepared by electrospinning combined with double-crucible method. X-ray powder diffraction (XRD) analysis indicates that $La_2O_2S:Tb^{3+}$ nanobelts were pure hexagonal phase with space group P-3m1. Scanning electron microscope (SEM) analysis reveals that $La_2O_2S:Tb^{3+}$ nanobelts have coarse surface with the mean width of 2.86±0.39 μm. Photoluminescence (PL) analysis manifests that $La_2O_2S:Tb^{3+}$ nanobelts emitted green emission at 544 nm attributed to $^5D_4 \rightarrow ^7F_5$ energy levels transition of Tb^{3+} ions. CIE analysis demonstrated that the emitting colors of $La_2O_2S:Tb^{3+}$ nanobelts were located in the green region and color-tuned luminescence can be obtained by changing doping concentration of Tb^{3+} ions, which is considered to be a promising candidate for application in LEDs. The possible formation mechanism of $La_2O_2S:Tb^{3+}$ nanobelts was also proposed. More importantly, the design conception and construction technology are of universal significance to fabricate other oxysulfides nanobelts.

1. Introduction

The lanthanide (La-Lu) oxysulfides are known as wide-gap (4.6-4.8 eV) materials suitable for doping ions activation [1-3]. In addition, compared with the lanthanide oxides, oxysulfide is a more efficient phosphor with a broader excitation band. Therefore, the lanthanide oxysulfides become a very important host of inorganic materials which have high potential for applications in various fields, such as color television picture tubes, radiographic imaging, field emission displays, and long-lasting phosphorescence [4-6]. RE oxysulfides are more biocompatible than RE oxide, may be used as biological probe and label. Various routes have been explored to synthesize such useful materials. Conventionally, Ln_2O_2S (Ln=Y, La, Gd) were prepared by combustion reactions from mixed metal nitrate reactants and dithiooxamide $(CSNH_2)_2$ with ignition temperatures of 300-350 °C [7]. Pure-phase nanowires of Ln_2O_2S, $Ln_2O_2S_2$, and LnS_2 have been prepared through shape retention of the same starting $Ln(OH)_3$ (Ln=La or Nd) nanowires *via* a boron-sulfur method at 400-500 °C for 10 min or 24 h [8]. $La_2O_2S:Yb$, Er phosphors could be synthesized by calcining the mixture of rare-earth oxides with S at 1200 °C [9].

In recent years, nanomaterials have been extensively studied because of their distinctive geometries, novel physical and chemical properties, and potential applications in nanoscale optical and electric devices [10-12]. Among these nanomaterials, nanobelt is a new kind of one-dimensional nanomaterials with special morphology [13-15]. It has attracted increasing interest of scientists owing to its anisotropy, large width-to-thickness ratio, unique optical, electrical and magnetic performances [16-19]. Research on the fabrication and properties of nanobelts has become one of the popular subjects of study in the realm of nanomaterials.

Currently, electrospinning has been found to be an effective route to various compounds. Electrospinning is a technique that allows fabrication of continuous fibers with diameters ranging from tens of nanometers up to micrometers [20, 21]. The morphology of materials can be controlled by adjusting experimental conditions, such as the viscosity of spinning solution, relative air humidity, the structure of spinneret, spinning voltage, and the distance between the spinneret and the collector. Electrospun nanomaterils have already found use in applications that include ultrafiltration, tissue engineering, catalysis, as well as fabrication of solar cells, transistors, sensors, memories, and many other types of devices [22, 23]. Advantages of

this novel process for fabricating 1D nanostructures include, but is not limited to, low cost, high efficiency and convenient assembly.

In order to verify the effectiveness of this experimental method, we have been fabricated a series of La_2O_2S nanomaterials *via* electrospinning combined with double-crucible method. But each sample has its own characteristics in the preparation process, and it is not a simple repetitive work. Such as $La_2O_2S:Eu^{3+}$ hollow nanofibers [24] were obtained by using different experimental parameters from this paper, such as, PVP (K15, Mw=10 000, AR), positive high voltage. It is the theoretical and experimental basis of this paper. In this study, pure hexagonal phase $La_2O_2S:Tb^{3+}$ nanobelts were prepared through calcining the electrospun PVP/[$La(NO_3)_3$+$Tb(NO_3)_3$] composite nanobelts, and then $La_2O_2S:x\%Tb^{3+}$[x stands for molar ratio of Tb^{3+} to (La^{3+}+Tb^{3+}), x=1, 3, 5 and 7] nanobelts were fabricated by sulfurization of $La_2O_3:x\%Tb^{3+}$ nanobelts *via* a double-crucible method. The samples were systematically characterized using modern measurements techniques. A possible formation mechanism of $La_2O_2S:Tb^{3+}$ nanobelts was also presented and some meaningful results were obtained.

2. Experimental sections

2.1. Chemicals

Polyvinyl pyrrolidone (PVP) (K90, Mw=90 000, AR) was bought from Tiantai Chemical Co. Ltd. Yttrium oxide (La_2O_3, 99.99%) and terbium oxide (Tb_4O_7, 99.99%) were purchased from Kemiou Chemical Co.,Ltd. N, N-dimethylformamide (DMF, AR) and Sulfur powder (S, AR) were purchased from Sinopharm Chemical Reagent Co. Ltd. Nitric acid (HNO_3, AR) was bought from Beijing Chemical Works. All chemicals were directly used as received without further purification.

2.2. Preparation of PVP/[$La(NO_3)_3$+$Tb(NO_3)_3$] composite nanobelts *via* electrospinning

In the typical procedure of preparing $La_2O_3:5\%Tb^{3+}$ nanobelts, 1.140 g of La_2O_3 and 0.069 g of Tb_4O_7 were dissolved in dilute HNO_3 at elevated temperatures to form $RE(NO_3)_3 \cdot 6H_2O$ (RE=La^{3+} and Tb^{3+}). The rare earth nitrates were dissolved in 13.600 g of DMF, and then 4.000 g of PVP was added into the above solution. The solution was magnetically stirred for 10 h to form homogeneous transparent precursor solution. In the spinning solution, the mass ratios of rare earth nitrates, DMF and PVP were equal to 12:68:20. Subsequently, the precursor solution was electrospun at room temperature under a positive high voltage of 8 kV, the distance between the capillary tip and the collector (Aluminium foil) was fixed to 20 cm, and relative humidity was

40%-60%. PVP/[$La(NO_3)_3$+$Tb(NO_3)_3$] composite nanobelts were obtained on the collector. Other series of $La_2O_3:x\%Tb^{3+}$ (x=1, 3 and 7) nanobelts were prepared by the similar procedure except for different doping molar concentration of Tb^{3+}.

2.3. Fabrication of $La_2O_3:Tb^{3+}$ nanobelts

The above PVP/[$La(NO_3)_3$+$Tb(NO_3)_3$] composite nanobelts were calcined at 700 ℃ for 8 h with a heating rate of 1 ℃/min. Then the calcination temperature was decreased to 200 ℃ at a rate of 1 ℃/min. Finally, samples were naturally cooled down to room temperature and $La_2O_3:Tb^{3+}$ nanobelts were obtained.

2.4. Synthesis of $La_2O_2S:Tb^{3+}$ nanobelts

$La_2O_3:Tb^{3+}$ nanobelts were loaded into a small crucible. A few carbon rods were put into a big crucible, and then the small crucible was placed into the big crucible. Next, some sulphur powders were loaded into the space between the two crucibles, and then the big crucible was covered with its lid. We call this process a double-crucible method. Finally the crucibles were annealed at 800 ℃ for 4 h under argon atmosphere, and then the temperature was decreased to 200 ℃ at a rate of 1 ℃/min followed by natural cooling down to ambient temperature. Thus, $La_2O_2S:Tb^{3+}$ nanobelts were obtained.

2.5. Characterization methods

The X-ray diffraction (XRD) measurement was performed using a Rigaku D/max-RA XRD diffractometer with Cu Kα line of 0.15418 nm. The field emission scanning electron microscope (FESEM, XL-30, FEI Company) was used to characterize the morphologies and sizes of the products. The distribution histograms of diameters were drawn by Image-Pro Plus 6.0 and origin 8.5 softwares. The excitation and emission spectra of samples were recorded with a HITACHI F-7000 fluorescence spectrophotometer using a Xe lamp as the excitation source.

3. Results and discussion

3.1. Characterizations of structure and morphology

Fig. 1 reveals the XRD patterns of $La_2O_2S:Tb^{3+}$ nanobelts. The XRD analysis result of $La_2O_2S:Tb^{3+}$ nanobelts demonstrates that the characteristic diffraction peaks of the samples can be easily indexed to those of the pure hexagonal phase with primitive structure of La_2O_2S

(PDF#71-2098), and the space group is P-3m1. In addition, with the increase of the concentration of Tb^{3+}, no obvious shifting of peaks can be detected, indicating that La^{3+} may be substituted by Tb^{3+} successfully to form the luminescence center because of the similar radius between La^{3+} and Tb^{3+}. No peaks of any other phases or impurities are also detected, indicating that crystalline $La_2O_2S:Tb^{3+}$ were acquired *via* sulfurization of crystalline $La_2O_3:Tb^{3+}$.
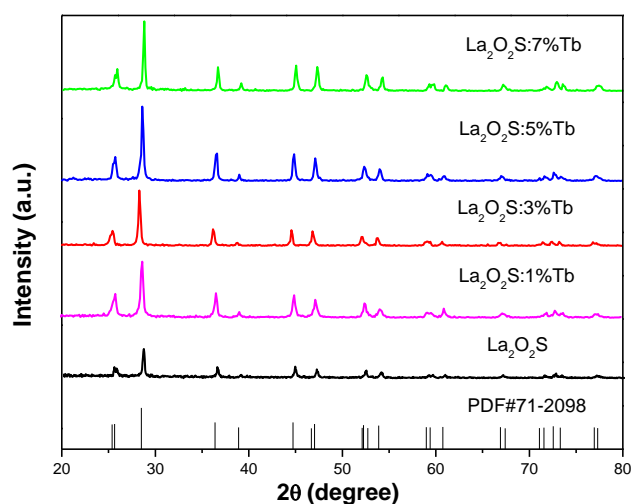
Fig. 1. XRD patterns of $La_2O_2S:x\%Tb^{3+}$ (x=0, 1, 3, 5 and 7) nanobelts (color online)

Fig. 2 shows the representative SEM images of the PVP/[La(NO_3)_3+Tb(NO_3)_3] composite nanobelts, $La_2O_3:Tb^{3+}$ nanobelts and $La_2O_2S:Tb^{3+}$ nanobelts. From the SEM image of Fig. 2a, it can be noticed that the PVP/[La(NO_3)_3+Tb(NO_3)_3] composite nanobelts have uniform width and smooth surface. Fig. 2b indicates the SEM image of as-prepared $La_2O_3:Tb^{3+}$ nanobelts. After annealing the respective electrospun PVP/[La(NO_3)_3+Tb(NO_3)_3] composite nanobelts at 700°C, the widths and thickness of the nanobelts greatly decrease due to loss of the PVP and associated organic components, as-formed $La_2O_3:Tb^{3+}$ nanobelts have relatively smooth surface, as revealed in Fig. 2b. After annealing and sulfurization at 800 °C, as-formed $La_2O_2S:Tb^{3+}$ nanobelts have coarse surface and retain the ribbon-shaped structure, as revealed in Fig. 2c. It reveals that $La_2O_2S:Tb^{3+}$ nanobelts retain their 1D morphology. From above analyses, we can safely conclude that the sulfurization technique we proposed here can retain the morphology of the precursor nanobelts.

Under the 95 % confidence level, the widths of PVP/[La(NO_3)_3+Tb(NO_3)_3] composite nanobelts, $La_2O_3:Tb^{3+}$ nanobelts and $La_2O_2S:Tb^{3+}$ nanobelts analyzed by Shapiro-Wilk method are normal distribution. Distribution histograms of widths of the samples are indicated in Fig. 3. As seen from Fig. 3, the widths of PVP/[La(NO_3)_3+Tb(NO_3)_3] composite nanobelts,

$La_2O_3:Tb^{3+}$ nanobelts and $La_2O_2S:Tb^{3+}$ nanobelts are 14.60 ± 1.83 µm, 3.29 ± 0.63 µm, and 2.86 ± 0.39 µm, respectively.
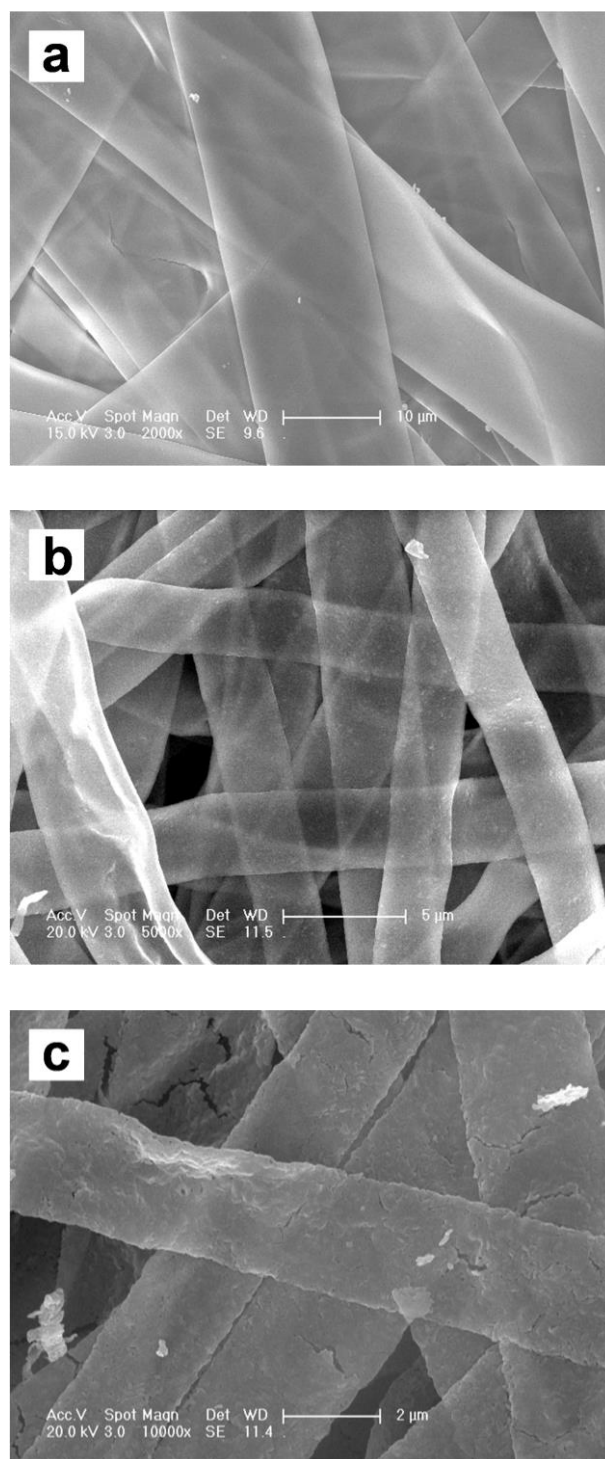
Fig. 2. SEM images of PVP/[La(NO_3)_3+Tb(NO_3)_3] composite nanobelts (a), $La_2O_3:Tb^{3+}$ nanobelts (b) and $La_2O_2S:Tb^{3+}$ nanobelts (c)
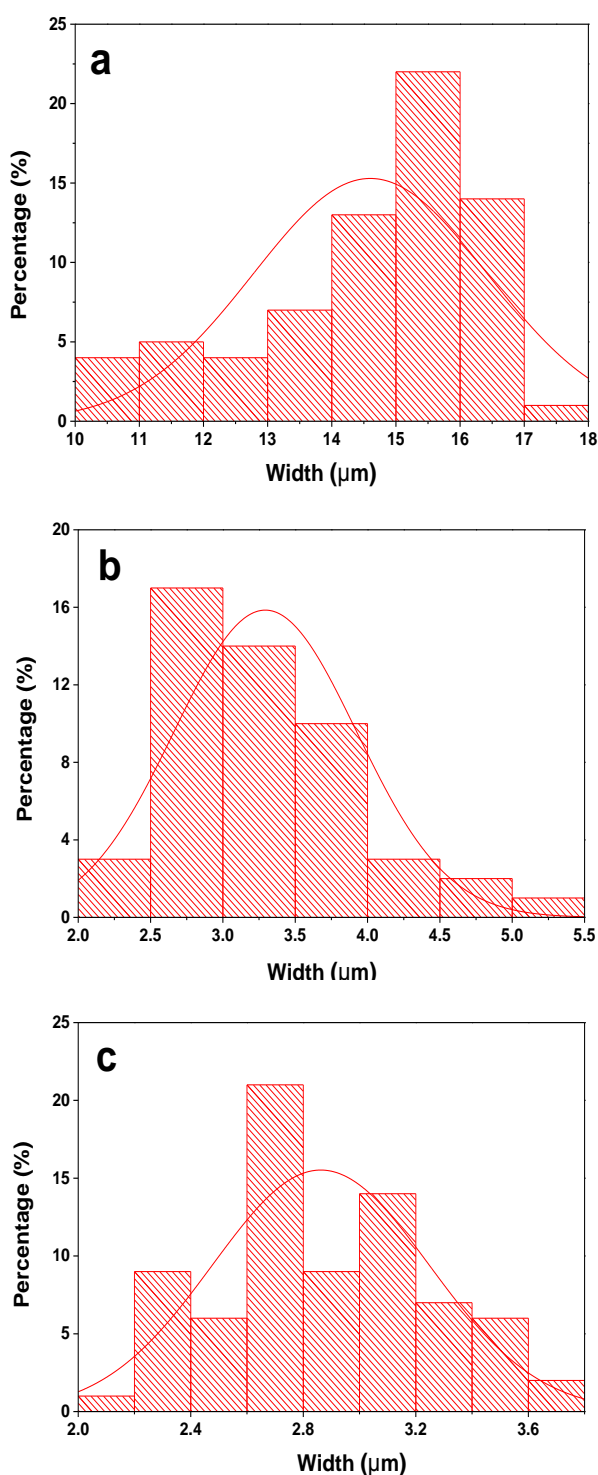
Fig. 3. Distribution histograms of widths of PVP/[La(NO₃)₃+Tb(NO₃)₃] composite nanobelts (a), La₂O₃:Tb³⁺ nanobelts (b) and La₂O₂S:Tb³⁺ nanobelts (c) (color online)

3.2. Photoluminescence properties

Fig. 4 shows the excitation (monitored by 544 nm) and emission (excited by 260 nm) spectra of $La_2O_2S:x\%Tb^{3+}$ (x=1, 3, 5 and 7) nanobelts. The excitation spectra (Fig. 4a) exhibits one strong broadband in the range from 200 to 300 nm with a maximum at 260 nm,

which is attributed to transition of the electron ground state to the split 5d energy levels, namely $4f^8 \rightarrow 4f^7 5d^1$ energy levels transitions of Tb^{3+} [6]. The emission spectra of $La_2O_2S:x\%Tb^{3+}$ (x=1, 3, 5 and 7) nanobelts is shown in the Fig. 4b. It is found from Fig. 7b that the green emission peaks consist of two main peaks at 489 nm and 544 nm, which originate from $^5D_4 \rightarrow ^7F_J$ (J=6 and 5) energy levels transitions of Tb^{3+} ions, respectively. The weak emission peak at 587 nm is ascribed to the $^5D_4 \rightarrow ^7F_4$ energy level transitions of Tb^{3+} ions. Among these emission peaks, the green emission at 544 nm attributed to $^5D_4 \rightarrow ^7F_5$ energy levels transition of Tb^{3+} ions is the strongest one.

Fig. 4 demonstrates the PL spectra of $La_2O_2S:Tb^{3+}$ nanobelts with different doping concentrations of Tb^{3+} ions. It is found that the spectral shape and locations of excitation and emission peaks do not vary with the doping concentrations of Tb^{3+} ions for $La_2O_2S:Tb^{3+}$ nanobelts, but the intensity of excitation and emission peaks for $La_2O_2S:Tb^{3+}$ nanobelts strongly depend on the doping concentration of Tb^{3+} ions, and the strongest excitation and emission spectra can be obtained when the doping molar concentration of Tb^{3+} is 5%. Obviously, the luminescence intensity of $La_2O_2S:Tb^{3+}$ nanobelts increases with the increase of the concentration of Tb^{3+} from the beginning, reaches a maximum value with the Tb^{3+} concentration of 5%, and then decreases with further increase in Tb^{3+} concentration.
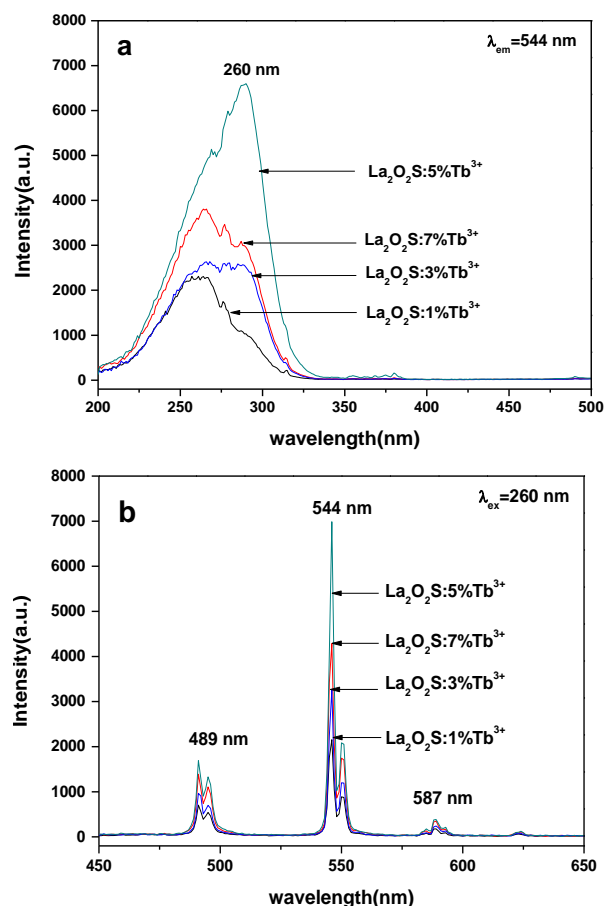

Fig. 4. Excitation (a) and emission (b) spectra of the La₂O₂S:x%Tb³⁺ (x=1, 3, 5 and 7) nanobelts (color online)

3.3. CIE analysis

Generally, color is represented by the Commission Internationale de L'Eclairage (CIE) chromaticity coordinates and color ratios. The chromaticity coordinates and color ratios have been calculated from the emission spectra by the method described in previous report [17, 18]. For the La$_2$O$_2$S:x%Tb^{3+} (x=1, 3, 5 and 7) nanobelts, the chromaticity coordinates (X, Y) are determined to be (0.3096，0.6784), (0.2916，0.6502), (0.2618，0.6122) and (0.2246,0.5728), respectively. Remarkably, the emission colors of La$_2$O$_2$S:x%Tb^{3+} (x=1, 3, 5 and 7) nanobelts with the variation of concentrations of Tb^{3+} are shown in Fig.5. These results indicate that the color emissions can be tuned by changing the concentration of doping activator ions. These as-obtained nanostructures could show merits of green emissions, which is applied in the field of optical telecommunication and optoelectronic devices.
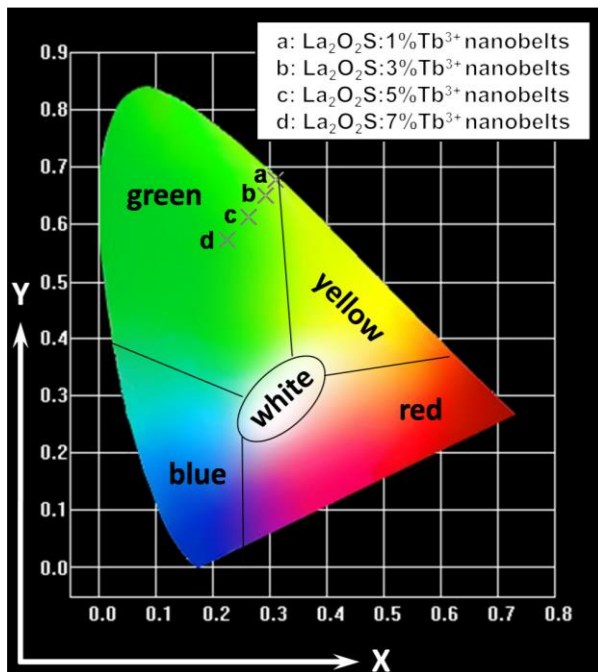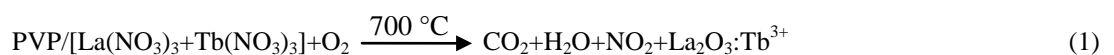

Fig. 5. CIE chromaticity coordinates diagram of La$_2$O$_2$S:x%Tb^{3+} (x=1, 3, 5 and 7) nanobelts (color online)

3.4. Formation mechanism for La$_2$O$_2$S:Tb^{3+} nanobelts

The formation mechanism for La$_2$O$_2$S:Tb^{3+} nanobelts is proposed on the basis of the above experiment results, as shown in Fig.6. PVP, La(NO$_3$)$_3$ and Tb(NO$_3$)$_3$ were mixed with DMF to form precursor solution with certain viscosity. Then, PVP/[La(NO$_3$)$_3$+Tb(NO$_3$)$_3$] composite nanobelts were obtained *via* electrospinning. Because the viscosity of the spinning solution for preparing nanobelts was higher, and the applied voltage was lower, so that the spinning velocity was slower. The charge repulsion force had adequate time to stretch the jets into belt shape, led to the formation of composite nanobelts. The morphologies of the composite nanostructures were basically retained after performing the following calcination process. Some solvent was volatilized in the electrospinning process. During calcination process, PVP chain was broken and volatilize. The La^{3+}, Tb^{3+} and NO$_3^-$ ions moved to the surface of the composite belts with evaporation of solvent DMF. With the increase in calcination temperature, nitrates were decomposed and oxidized to NO$_2$, La^{3+} and Tb^{3+} were oxidized to form La$_2$O$_3$:Tb^{3+} crystallites, many crystallites were combined into nanoparticles, then some nanoparticles were mutually connected to generate La$_2$O$_3$:Tb^{3+} nanobelts. PVP acted as template during the formation of La$_2$O$_3$:Tb^{3+} nanobelts. It was found from experiments that the average molecular weight of PVP and content of PVP in the precursor solution played important roles in the formation of La$_2$O$_3$:Tb^{3+} nanobelts [2]. Next, La$_2$O$_3$:Tb^{3+} nanobelts were sulfurized using sulfur powders as sulfurizing agent. During the process, sulfur powders and La$_2$O$_3$:Tb^{3+} nanobelts were separated by the small crucible, which prevented La$_2$O$_3$:Tb^{3+} nanobelts from morphology damage. If La$_2$O$_3$:Tb^{3+} nanobelts were directly mixed with sulfur powders, melted sulfur will cut the La$_2$O$_3$:Tb^{3+} nanobelts into pieces, as a result, the morphology of La$_2$O$_3$:Tb^{3+} nanobelts cannot be retained [17]. Carbon rods played an important role in the reduction *via* combination with O$_2$ to produce CO, which react with oxygen species of La$_2$O$_3$:Tb^{3+} to give CO$_2$ in the heating process. The double-crucible method we proposed here is actually a solid-gas reaction, which has been proved to be an important method, not only can retain the morphology of La$_2$O$_3$:Tb^{3+} nanobelts, but also can fabricate La$_2$O$_2$S:Tb^{3+} nanobelts with pure phase at relatively low temperature. Reaction schemes for formation of La$_2$O$_2$S:Tb^{3+} nanobelts proceed as follows:
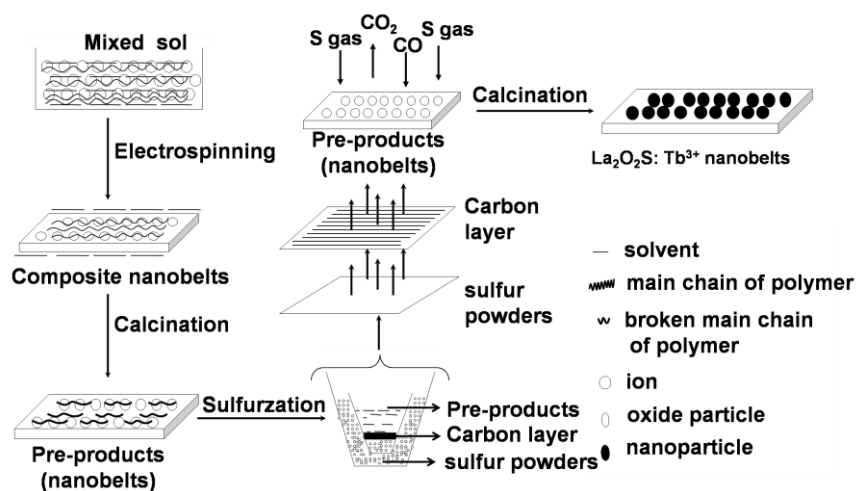
$$PVP/[La(NO_3)_3+Tb(NO_3)_3]+O_2 \xrightarrow{700\ ^\circ C} CO_2+H_2O+NO_2+La_2O_3:Tb^{3+} \qquad (1)$$

$$C+O_2 \longrightarrow CO \qquad (2)$$

$$La_2O_3:Tb^{3+}+S+CO \xrightarrow{800\ ^\circ C} La_2O_2S:Tb^{3+}+CO_2 \qquad (3)$$

Fig. 6. Formation mechanism of $La_2O_2S:Tb^{3+}$ nanobelts

4. Conclusions

In summary, pure hexagonal phase $La_2O_2S:Tb^{3+}$ nanobelts with space group P-3m1 were fabricated *via* sulfurization of the $La_2O_3:Tb^{3+}$ nanobelts. The morphology of $La_2O_2S:Tb^{3+}$ nanobelts can be inherited from $La_2O_3:Tb^{3+}$ nanobelts under the sulfurization circumstance *via* a double-crucible method we newly proposed. The widths of $La_2O_2S:Tb^{3+}$ nanobelts analyzed by Shapiro-Wilk method are normal distribution and are $2.86 \pm 0.39 \mu m$. Emission spectra analysis manifested that $La_2O_2S:Tb^{3+}$ nanobelts emitted green emission at 544 nm attributed to $^5D_4 \rightarrow {}^7F_5$ energy levels transition of Tb^{3+} ions. The double-crucible method we proposed here is of great importance. This technique can be employed to fabrication of other pure-phase rare earth oxysulfide nanomaterials with various morphologies.

References

[1] G. D. Liu, Q. H. Zhang, H. Z. Wang, Y. G. Li, Mater. Sci. Eng. B **177**, 316 (2012).
[2] L. Y. Yang, J. X. Wang, X. T. Dong, G. X. Liu, W. S. Yu, J. Mater. Sci. **48**, 644 (2013).
[3] M. Pokhrel, A. K. Gangadharan, D. K. Sardar, Mater. Lett. **99**, 86 (2013).
[4] N. T. Lau, M. Fang, C. K. Chan, Appl. Catal. B: Environ. **79**, 110 (2018).
[5] Y. M. Yang, C. Mi, F. Yu, X. Y. Su, C. F. Guo, G. Li, J Zhang, L. L. Liu, Y. Z. Liu, X. D. Li, Ceram. Int. **40**, 9875 (2014).
[6] S. V. Yap, R. M. Ranson, W. M. Cranton, D. C. Koutsogeorgis, G. B. Hix, J. Lumin. **129**, 416 (2009).
[7] J. Bang, M. Abboudi, B. Abrams, P. H. Holloway, J. Lumin. **106**, 177 (2004).
[8] Y. Z. Huang, L. Chen, L. M. Wu, Cryst. Growth Des. **8**(2), 739 (2008).
[9] J. J. Oh, B. K. Jin, W. J. Chung, D. W. Shin, Y. G. Choi, Curr. Appl. Phys. **11**, S15 (2011).
[10] M. Q. Chi, S. H. Chen, M. X. Zhong, C. Wang, X. F. Lu, Chem. Commun. **54**, 5827 (2018).
[11] Y. T. Geng, P. Zhang, Q. T. Wang, Y. X. Liu, K. Pan, J. Mater. Chem. B **5**, 5390 (2017).
[12] C. Luo, X. X. Wang, J. Q. Wang, K. Pan, Compos. Sci. Technol. **133**, 97 (2016).
[13] N. Lv, Z. Q. Wang, W. Z. Bi, G. M. Li, J. L. Zhang, J. Z. Ni, J. Mater. Chem. B **4**, 4402 (2016).
[14] M. Gao, X. F. Lu, M. Q. Chi, S. H. Chen, C. Wang, Inorg. Chem. Front. **4**, 1862 (2017).
[15] N. Lv, J. L. Zhang, G. M. Li, X. Wang, J. Z. Ni, J. Phys. Chem. C **121**(21), 11926 (2017).
[16] Q. L. Ma, J. X. Wang, X. T. Dong, W. S. Yu, G. X. Liu, Adv. Funct. Mater. **25**(16), 2436 (2015).
[17] W. W. Ma, X. T. Dong, J. X. Wang, W. S. Yu, G. X. Liu, J. Mater. Sci. **48**, 2557 (2013).

[18] K. Lun, Q. L. Ma, M. Yang, X. T. Dong, Y. Yang, J. X. Wang, W. S. Yu, G. X. Liu, Chem. Eng. J. **279**, 231 (2015).

[19] J. Tian, Q. L. Ma, W. S. Yu, X. T. Dong, Y. Yang, B. Zhao, J. X. Wang, G. X. Liu, New J. Chem. **41**, 13983 (2017).

[20] X. F. Lu, C. Wang, Y. Wei, Small **5**, 2349 (2009).

[21] J. Zhao, Y. Yang, X. T. Dong, Q. L. Ma, W. S. Yu, J. X. Wang, G. X. Liu, RSC Advances **6**(69), 64741 (2016).

[22] S. Xu, X. L. Wang, X. T. Dong, W. S. Yu, J. X. Wang, G. X. Liu, RSC Advances **6**(49), 43322 (2016).

[23] S. L. Chen, H. Q. Hou, F. Harnisch, S. A. Patil, A. A. Carmona-Martinez, S. Agarwal, Y. Y. Zhang, S. Sinha-Ray, A. L. Yarin, A. Greiner, U. Schröder, Energy Environ. Sci. **4**, 1417 (2011).

[24] F. Bi, J. Q. Li, G. Q. Gai, X. T. Dong, J. Optoelectron. Adv. M. **22**(5-6), 272 (2020).

_____

*Corresponding author: wlynzy@163.com